Supplemental Material for "Giant-Atom Quantum Batteries"

Ke-Xiong Yan,[1,2] Yang Liu,[3] Yang Xiao,[1] Jun-Hao Lin,[1]
Jie Song,[4] Ye-Hong Chen,[1,2,5,*] Franco Nori,[2,6] and Yan Xia[1,5,†]

[1] *Fujian Key Laboratory of Quantum Information and Quantum Optics, College of Physics and Information Engineering, Fuzhou University, Fuzhou 350108, China*
[2] *Quantum Information Physics Theory Research Team, Center for Quantum Computing, RIKEN, Wako-shi, Saitama 351-0198, Japan*
[3] *Center for Joint Quantum Studies and Department of Physics, School of Science, Tianjin University, Tianjin 300350, China*
[4] *Department of Physics, Harbin Institute of Technology, Harbin 150001, China*
[5] *Institute of Quantum Science and Technology, Yanbian University, Yanji 133002, China*
[6] *Department of Physics, University of Michigan, Ann Arbor, Michigan 48109-1040, USA*

(Dated: April 10, 2026)

S1. PERFORMANCE METRICS AND ROBUSTNESS

A. Maximum ergotropy and maximum power in three configurations

From Fig. S1, we can find that the charging properties of the separated configuration and the nested configuration exhibit similar shapes. The charging characteristics of both configurations vary with the phase shift, exhibiting a period of 2π. The braided configurations are different in that their charging characteristics vary with phase shift over a period of π. When the phase shift θ is between 0 and $\pi/3$ or between $5\pi/3$ and 2π, the nested configuration exhibits superior charging characteristics. This is because, during these phase intervals, both the individual dissipation rate and collective dissipation rate of the nested configuration are lower than those of the other two configurations. However, during other phase intervals, the charging characteristics of the braided configuration are better than the separated configuration and the nested configuration. We also observe that the maximum energy of the braided configuration is ω_0 when $\theta = \pi/2$, which makes wireless charging over long distances possible. The batteries composed of the separated configurations and the nested configuration are not suitable for energy storage and long-distance transmission because of the aging problem. However, since separated giant-atoms (GAs) and nested GAs can decouple from the waveguide at a phase of π, this property might be useful as an energy terminator, i.e., to block the transmission of energy between two GAs.

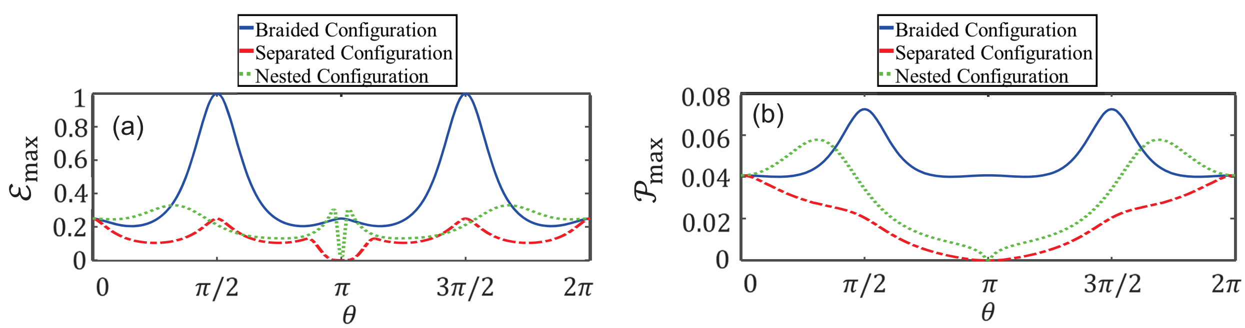

FIG. S1. (a) Maximum ergotropy $\mathcal{E}_{\max}$ and (b) maximum power $\mathcal{P}_{\max}$ as functions of θ for the braided, separated, and nested configuration.

* yehong.chen@fzu.edu.cn
† xia-208@163.com

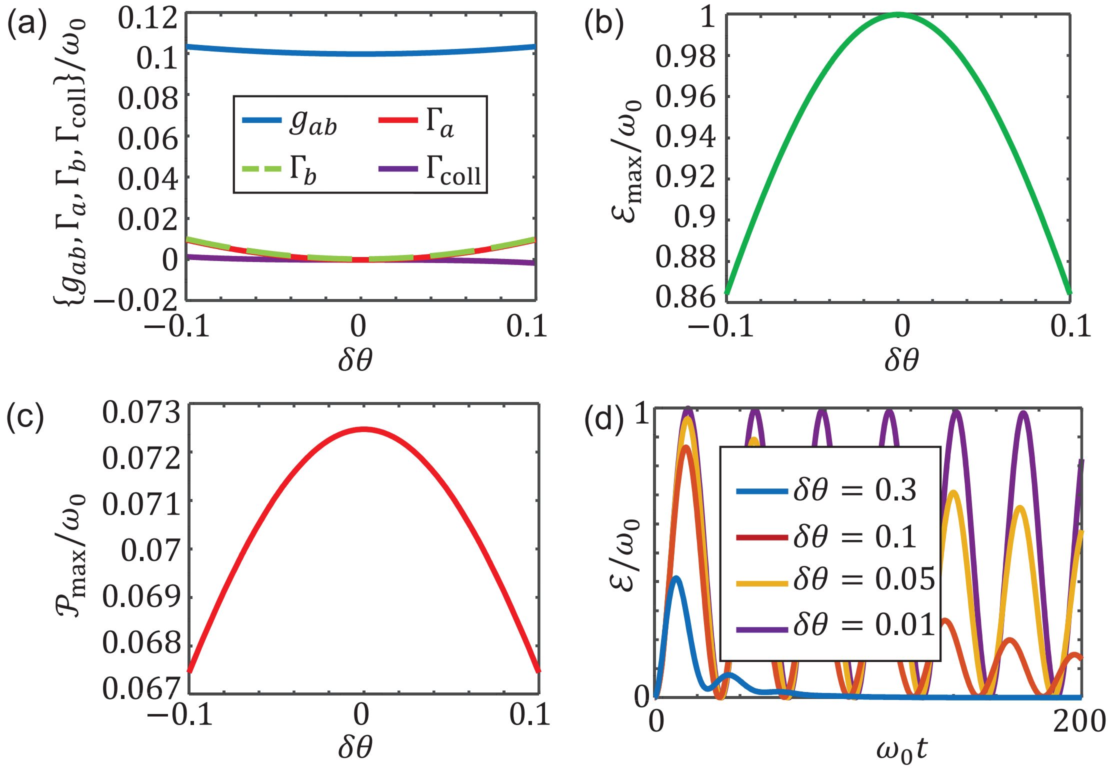

FIG. S2. Effect of phase deviation on (a) the exchange interaction, individual dissipation rate, and collective dissipation rate; (b) the maximum ergotropy; and (c) the maximum power. (d) The charging process of the braided GAs under various phase deviations.

B. Robustness to phase deviations

In the braided configuration, realizing a decoherence-free interaction requires satisfying the phase condition, namely $\theta = (n + 1/2)\pi$ $(n = 1, 2, 3, \ldots)$. To better bridge the gap between theory and experiment, we discuss the charging performance of the braided-GA quantum battery (QB) when phase deviations are present. We define the phase deviation rate as $\delta\theta = (\theta - \pi/2)/(\pi/2)$. In Fig. S2(a), we plot the variation of the exchange coupling strength g_{ab}, individual dissipation rates $\Gamma_{a(b)}$, and collective dissipation rate $\Gamma_{\rm coll}$ as a function of the phase deviation rate within the range of 0.1. It can be observed that when the phase deviation rate is less than 0.1, the collective dissipation rate is nearly zero, the individual dissipation rate is less than $0.01\omega_0$, and the exchange interaction is almost stable at $0.1\omega_0$. This indicates that the deviation from the phase mismatching has a greater impact on the individual dissipation rate. In Figs. S2(b) and (c), we plot the variation of the battery maximum ergotropy and maximum charging power with respect to the phase deviation. When the phase deviation rate is less than 0.1, the maximum ergotropy is greater than $0.86\omega_0$, and the maximum charging power is above $0.0675\omega_0$. The battery charging curves under various phase deviations are presented in Fig. S2(d). It can be seen that when the deviation rate is less than 0.01, the braided-GA QB can still perform nearly lossless energy exchange.

S2. GAS QB CHARGED BY CAVITY

A. Two braided GAs

We treat the two braided GA as battery medium and additionally introduce a microwave cavity as a charger. The microwave cavity interacts with only one GA, thereby preventing any contamination of the charging efficiency from interatomic interactions. For simplicity, we first neglect the dissipation of the single-mode cavity field and leave the two braided GAs in the sweet spot (i.e. $\theta = \pi/2$). The Hamiltonian of this QB model can be written as

$$H_s = H_B + H_C + H_I, \tag{S1}$$

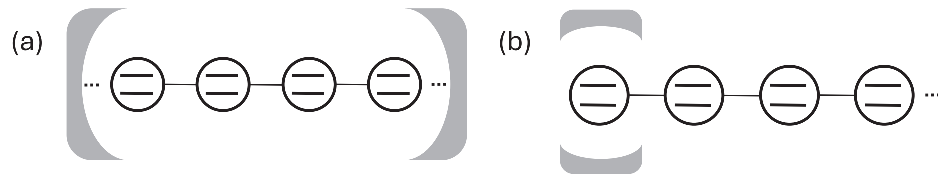

FIG. S3. (a) Schematic of a single-mode cavity coupled to all atoms in a one-dimensional spin chain. (b) Schematic of a single-mode cavity coupled to the first atom in a one-dimensional spin chain.

where H_B, H_C, and H_I represent the Hamiltonians of the GAs battery, the cavity charger, and the interaction terms, respectively, with the following forms (hereafter set $\hbar = 1$):

$$H_B = \frac{\omega_0}{2}(\sigma_a^z + \sigma_b^z) + \lambda_1(\sigma_a^+\sigma_b^- + \sigma_a^-\sigma_b^+), \tag{S2}$$

$$H_C = \omega_c a^\dagger a, \tag{S3}$$

$$H_I = \lambda_2(a^\dagger\sigma_a^- + a\sigma_a^+). \tag{S4}$$

Here, a and $a^\dagger$ are the annihilation and creation operators for the single-mode cavity of frequency ω_c. The Pauli operators for the jth GA are denoted by σ_j^α ($\alpha = x,\, y,\, z$), and the corresponding ladder operators are $\sigma_j^\pm$. Parameter λ_1 denote the coupling strength between the two GAs. Parameter λ_2 represents the coupling strength between the GA a and the single-mode cavity.

To study the charging property in the whole state space of the two GAs, we can work in the collective state representation, where the GAs-battery system behaves as a single four-level system. The four eigenstates of the GAs-battery system are

$$\begin{aligned} |\psi_1\rangle &= \sqrt{2}(|g_a, e_b\rangle - |e_a, g_b\rangle)/2, \\ |\psi_2\rangle &= |g_a, g_b\rangle, \\ |\psi_3\rangle &= |e_a, e_b\rangle, \\ |\psi_4\rangle &= \sqrt{2}(|g_a, e_b\rangle + |e_a, g_b\rangle)/2 \end{aligned}$$

with the corresponding eigenenergies $E_1 = -\lambda_1$, $E_2 = -\omega_0$, $E_3 = \omega_0$, and $E_4 = \lambda_1$. In this representation, the Hamiltonian of the system can be rewritten as

$$H_s = J_z + \omega_c a^\dagger a + \lambda_2(a^\dagger J_- + \text{H.c.}), \tag{S5}$$

where

$$\begin{aligned} J_z &= -\lambda_1 |\psi_1\rangle\langle\psi_1| - \omega_0 |\psi_2\rangle\langle\psi_2| + \omega_0 |\psi_3\rangle\langle\psi_3| + \lambda_1 |\psi_4\rangle\langle\psi_4|, \\ J_- &= \sqrt{2}(-|\psi_2\rangle\langle\psi_1| + |\psi_1\rangle\langle\psi_3| + |\psi_4\rangle\langle\psi_3| + |\psi_2\rangle\langle\psi_4|)/2. \end{aligned}$$

When the conditions $\omega_c = \omega_0$ and $\lambda_1 \ll \lambda_2$ are satisfied, the system dynamics is described by the following effective Hamiltonian [S1]:

$$H_s^{\text{eff}} = \frac{\lambda_2^2}{\lambda_1}\left[(a^\dagger a + \frac{1}{2})(|\psi_4\rangle\langle\psi_4| - |\psi_1\rangle\langle\psi_1|) - (a^\dagger)^2 |\psi_2\rangle\langle\psi_3| - a^2 |\psi_3\rangle\langle\psi_2|\right]. \tag{S6}$$

The above Hamiltonian describes the dynamics of two GAs excited simultaneously by two photons, a process in which interatomic interactions are waveguide-mediated and decoherence-immune. When charging is complete, the interaction between the cavity and the first GA is cut off, and the energy can be stored losslessly in the two braided GAs.

B. 1D spin chain consisting of N braided GAs

We consider N braided GAs as battery medium and introduce a microwave cavity as a charger. N braided GAs coupled to a waveguide form a one-dimensional spin chain. In contrast to capacitance-mediated atomic chains, waveguide-mediated atomic chains do not have next-nearest-neighbor crosstalk. Furthermore, in standard circuit-QED setups, the presence of the dispersive regime limits the efficiency of energy transfer between batteries, whereas giant-atom waveguide systems are free from such theoretical constraints. Specifically, the circuit-QED paradigm typically requires the qubits and the mediator to operate in the dispersive regime (large detuning $\Delta \ll g$), which inherently results in a significantly attenuated effective interaction (g^2/Δ). This second-order process inevitably limits the efficiency and charging power of the energy exchange between the qubits. In contrast, for braided GAs operating under a decoherence-free coupling mechanism, the effective interaction strength is directly determined by the individual relaxation rate (γ). Consequently, the waveguide-mediated interaction between GAs, characterized by a resonant first-order process, is theoretically more robust than the second-order interaction mediated by discrete-mode couplers.

Two distinct charging protocols are explored: (1) collective charging, where the cavity couples to all GAs, and (2) single-atom charging, where the cavity interacts solely with the first GA in the chain simultaneously.

(1) Collective Charging [see Fig. S3(a)]: The cavity interacts uniformly with all atoms in the spin chain. The corresponding system Hamiltonian is given by

$$H_1 \;=\; H_B + H_C + g(t)H_{Ic}, \tag{S7}$$

where the time-dependent parameter $g(t)$ defines the charging time interval. We assume $g(t)$ as a step function equal to 1 for $t \in [0,T]$ and zero elsewhere.

The operators H_B, H_C, and H_{Ic} represent the Hamiltonians of the 1D spin chain battery, charger, and interaction terms, respectively, with the following forms:

$$H_B \;=\; \frac{\omega_q}{2}\sum_{i=1}^{N}\sigma_i^z + \lambda_1\sum_{i=1}^{N-1}(\sigma_i^+\sigma_{i+1}^- + \sigma_i^-\sigma_{i+1}^+), \tag{S8}$$

$$H_C \;=\; \omega_c a^\dagger a, \tag{S9}$$

$$H_{Ic} \;=\; \frac{\lambda_2}{\sqrt{N}}(a^\dagger + a)\sum_{i=1}^{N}\sigma_i^x. \tag{S10}$$

Here, a and $a^\dagger$ are the annihilation and creation operators for the single-mode cavity of frequency ω_c. The Pauli spin operators for the ith GA are denoted by σ_i^α ($\alpha = x,\, y,\, z$), and the corresponding ladder operators are $\sigma_i^\pm$. The transition frequency between the ground state $|g\rangle$ and excited state $|e\rangle$ of individual GAs are ω_q. The nearest-neighbor exchange interaction strength is λ_1. The collective spin-cavity coupling strength is λ_2. The $1/\sqrt{N}$ scaling ensures a finite total interaction energy in the thermodynamic limit.

(2) Single-atom Charging [see Fig. S3(b)]: The cavity couples exclusively to the first atom in the spin chain. In this case, the system Hamiltonian is

$$H_2 \;=\; H_B + H_C + g(t)H_{Is}, \tag{S11}$$

where the Hamiltonian of interaction term is

$$H_{Is} \;=\; \lambda_2(a^\dagger + a)\sigma_1^x. \tag{S12}$$

Here, the cavity interacts only with the first atom in the chain ($i = 1$), with λ_2 now representing the local coupling strength. The absence of $1/\sqrt{N}$ scaling reflects the localized nature of the interaction, where energy transfer to the chain relies on spin-spin correlations mediated by λ_1.

Figure S4 illustrates the effect of the coupling strength between GAs in different protocols on the charging characteristics. In the weak coupling regime (i.e., $\lambda_1 \le \lambda_2$), both the maximum energy and average power of collective charging are significantly higher than those of single-atom charging. This is attributed to the cavity-induced many-body interactions present in the collective charging protocol. This interaction strength enhances the charging power of the battery. In contrast, such many-body interactions are absent in the single-atom charging protocol, and the coupling strength between the GAs is insufficient to facilitate a rapid energy transfer. Under the strong coupling mechanism, both the maximum energy and average power of the single-atom charging protocol increase, surpassing those of the collective charging protocol. The strong interactions between the GAs disrupt the cavity-induced many-body interactions, resulting in a decline in the performance of the collective charging protocol. At the same time, these interactions accelerate the energy transfer rate in the single-atom charging protocol, causing its performance to

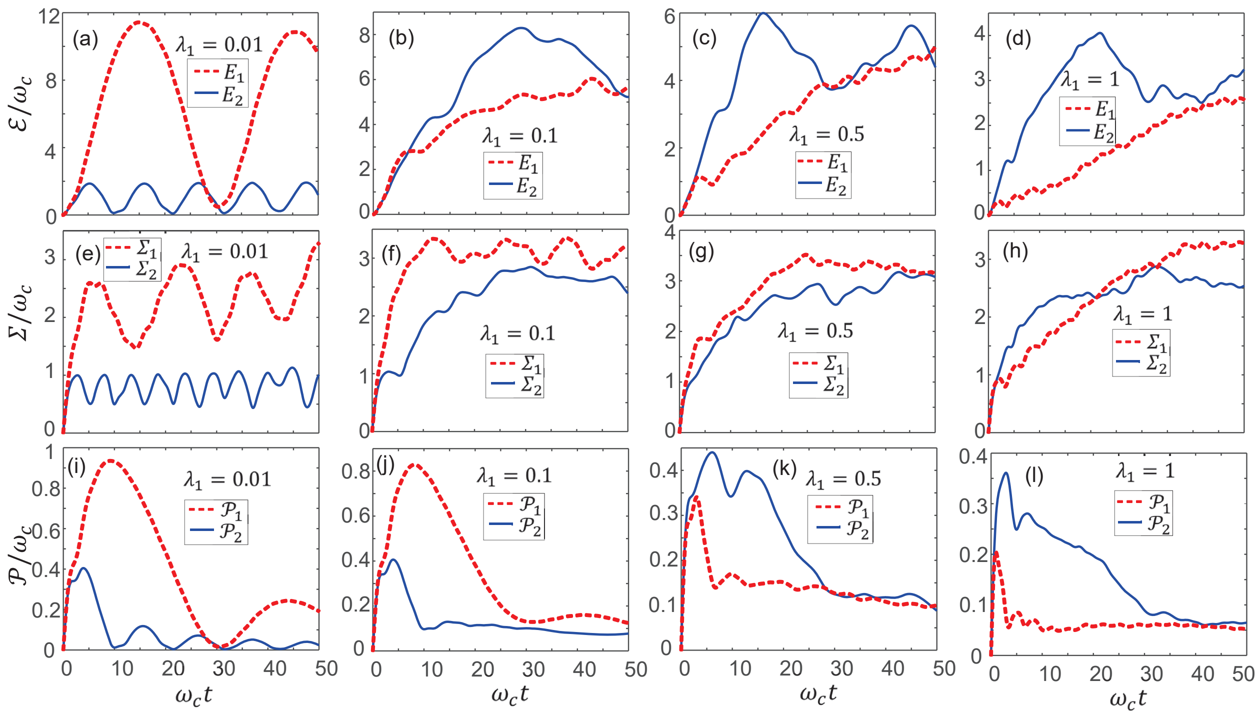

FIG. S4. (a)-(d) The dependence of the stored energy $E(t)$ (in units $\hbar\omega_c$), (e)-(h) energy quantum fluctuations $\sum(t)$ (in units $\hbar\omega_c$), and (i)-(l) average charging power $\mathcal{P}(t)$ ($\hbar\omega_c^2$) as a function of $\omega_c t$ for different coupling strength λ_1. The different curves in these plots stand for various charging protocols (red dashed line for Collective Charging and blue solid line for Single-atom Charging), and all are for a QB with the number of GAs $N = 6$. The cavity-atom coupling strength λ_2 in both protocols is set to 0.1. We take ω_c as a dimensionless parameter and let $\omega_c = \omega_q = 1$.

exceed that of the collective charging protocol. In summary, the competition between the coupling strengths of the GAs and the coupling strengths between the cavity and the GAs leads to distinct charging characteristics for the two protocols.

S3. SLH FORMALISM FOR TWO GAS

To derive the cascaded master equation for multiple GAs interacting with a waveguide, the SLH formalism provides a convenient framework [S2, S3]. For an open quantum system with n input-output channels, the general form for an SLH triplets is $G = (\mathrm{S}, \mathrm{L}, H)$, where S is an $n \times n$ scattering matrix, L is the $n \times 1$ vector representing jump operators to the coupled channels, and H is the Hamiltonian of the system.

A. Braided GAs

For two braided GAs (see in Fig. S5), the SLH triplet of each coupling point is

$$\begin{aligned} G_{R,1}^{a(b)} &= \left(1, \sqrt{\frac{\gamma_1^{a(b)}}{2}}\sigma_-^{a(b)}, \frac{\omega_{a(b)}}{2}\sigma_z^{a(b)}\right), \\ G_{R,2}^{a(b)} &= \left(1, \sqrt{\frac{\gamma_2^{a(b)}}{2}}\sigma_-^{a(b)}, 0\right), \\ G_{L,1}^{a(b)} &= \left(1, \sqrt{\frac{\gamma_1^{a(b)}}{2}}\sigma_-^{a(b)}, 0\right), \\ G_{L,2}^{a(b)} &= \left(1, \sqrt{\frac{\gamma_2^{a(b)}}{2}}\sigma_-^{a(b)}, 0\right), \end{aligned} \tag{S13}$$

where $L(R)$ represents the left (right) propagating channel and $\gamma_i^{a(b)}$ is the bare relaxation rate at each connection point. Since the right and left channels are expressed independently, S and L are simplified as one component by setting $n = 1$. We consider the case that there is no relative phase between the two connection points of each GA, but only a cumulative phase caused by the propagation of the bosonic field. The distance between neighboring coupling points is assumed to be d, such that the propagation phase between two adjacent coupling points is $\theta = k_0 d$ (k_0 is wave number of the central bose modes emitted by the GAs). The SLH triplet for the right propagating field is derived form the series product relation

$$G_{\mathrm{R}} = G^{b}_{\mathrm{R},2} \lhd G_\theta \lhd G^{a}_{\mathrm{R},2} \lhd G_\theta \lhd G^{b}_{\mathrm{R},1} \lhd G_\theta \lhd G^{a}_{\mathrm{R},1}, \tag{S14}$$

where $\lhd$ represents the series product between two SLH triplets and $G_\theta = (e^{i\theta}, 0, 0)$. Using the following equation

$$G_2 \lhd G_1 = \Big(S_2 S_1,\ S_2 L_1 + L_2,\ H_1 + H_2 + O_2,\ \big[L_2^\dagger S_2 L_1 - L_1^\dagger S_2^\dagger L_2\big]\Big), \tag{S15}$$

we can obtain

$$\begin{aligned}
S_R &= e^{3i\theta}, \\
L_R &= \Big(e^{3i\theta}\sqrt{\frac{\gamma_1^a}{2}} + e^{i\theta}\sqrt{\frac{\gamma_2^a}{2}}\Big)\sigma_-^a + \Big(e^{2i\theta}\sqrt{\frac{\gamma_1^b}{2}} + \sqrt{\frac{\gamma_2^b}{2}}\Big)\sigma_-^b \\
H_R &= \Big(\frac{\omega_a}{2} + \frac{\sqrt{\gamma_1^a\gamma_2^a}}{4}\sin 2\theta\Big)\sigma_z^a + \Big(\frac{\omega_b}{2} + \frac{\sqrt{\gamma_1^b\gamma_2^b}}{4}\sin 2\theta\Big)\sigma_z^b \\
&\quad + \frac{1}{4i}\left\{\Big[\Big(e^{i\theta}\sqrt{\gamma_1^a\gamma_1^b} + e^{3i\theta}\sqrt{\gamma_1^a\gamma_2^b} + e^{i\theta}\sqrt{\gamma_2^a\gamma_2^b}\Big)\sigma_-^a\sigma_+^b + e^{i\theta}\sqrt{\gamma_1^b\gamma_2^a}\sigma_+^a\sigma_-^b\Big] - \text{H.c.}\right\},
\end{aligned} \tag{S16}$$

where L_R is the jump operator of the right propagating modes. The terms proportional to $\sqrt{\gamma_1^{a(b)}\gamma_2^{a(b)}}\sin 2\theta$ in H_R are the Lamb shifts. Similarly, the SLH triplet G_L describing coupling with the left propagating modes is written as

$$\begin{aligned}
S_L &= e^{3i\theta}, \\
L_L &= \Big(\sqrt{\frac{\gamma_1^a}{2}} + e^{2i\theta}\sqrt{\frac{\gamma_2^a}{2}}\Big)\sigma_-^a + \Big(e^{i\theta}\sqrt{\frac{\gamma_1^b}{2}} + e^{3i\theta}\sqrt{\frac{\gamma_2^b}{2}}\Big)\sigma_-^b, \\
H_L &= \Big(\frac{\sqrt{\gamma_1^a\gamma_2^a}}{4}\sin 2\theta\Big)\sigma_z^a + \Big(\frac{\sqrt{\gamma_1^b\gamma_2^b}}{4}\sin 2\theta\Big)\sigma_z^b \\
&\quad + \frac{1}{4i}\left\{\Big[\Big(e^{i\theta}\sqrt{\gamma_1^a\gamma_1^b} + e^{3i\theta}\sqrt{\gamma_1^a\gamma_2^b} + e^{i\theta}\sqrt{\gamma_2^a\gamma_1^b}\Big)\sigma_+^a\sigma_-^b + e^{i\theta}\sqrt{\gamma_1^b\gamma_2^a}\sigma_-^a\sigma_+^b\Big] - \text{H.c.}\right\}.
\end{aligned} \tag{S17}$$

The total SLH triplet is given by the concatenation product

$$G_{\text{total}} = G_R \boxplus G_L = \left(\begin{bmatrix} S_R & 0 \\ 0 & S_L \end{bmatrix},\ \begin{bmatrix} L_R \\ L_L \end{bmatrix},\ H_R + H_L\right), \tag{S18}$$

with the components

$$\begin{aligned}
S_{\text{total}} &= \begin{bmatrix} e^{3i\theta} & 0 \\ 0 & e^{3i\theta} \end{bmatrix}, \\
L_{\text{total}} &= \begin{bmatrix} \Big(e^{3i\theta}\sqrt{\frac{\gamma_1^a}{2}} + e^{i\theta}\sqrt{\frac{\gamma_2^a}{2}}\Big)\sigma_-^a + \Big(e^{2i\theta}\sqrt{\frac{\gamma_1^b}{2}} + \sqrt{\frac{\gamma_2^b}{2}}\Big)\sigma_-^b \\ \Big(\sqrt{\frac{\gamma_1^a}{2}} + e^{2i\theta}\sqrt{\frac{\gamma_2^a}{2}}\Big)\sigma_-^a + \Big(e^{i\theta}\sqrt{\frac{\gamma_1^b}{2}} + e^{3i\theta}\sqrt{\frac{\gamma_2^b}{2}}\Big)\sigma_-^b \end{bmatrix}, \\
H_{\text{total}} &= \Big(\frac{\omega_a}{2} + \frac{\sqrt{\gamma_1^a\gamma_2^a}}{2}\sin 2\theta\Big)\sigma_z^a + \Big(\frac{\omega_b}{2} + \frac{\sqrt{\gamma_1^b\gamma_2^b}}{2}\sin 2\theta\Big)\sigma_z^b \\
&\quad + \frac{1}{2}\Big[\Big(\sqrt{\gamma_1^a\gamma_1^b} + \sqrt{\gamma_2^a\gamma_1^b} + \sqrt{\gamma_2^a\gamma_2^b}\Big)\sin\theta + \sqrt{\gamma_1^a\gamma_2^b}\sin 3\theta\Big](\sigma_-^a\sigma_+^b + \sigma_+^a\sigma_-^b).
\end{aligned} \tag{S19}$$

If we assume equal relaxation rates at all coupling points ($\gamma_1^a = \gamma_2^a = \gamma_1^b = \gamma_2^b = \gamma$), we can obtain the Lamb shifts

$$\delta\omega_a = \delta\omega_b = \gamma \sin 2\theta, \tag{S20}$$

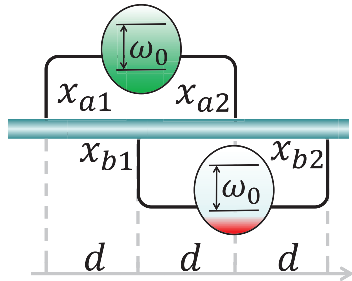

FIG. S5. Two braided GAs in the open waveguide.

the exchanging coupling strength

$$g_{ab} = \gamma(3\sin\theta + \sin 3\theta)/2, \tag{S21}$$

the individual decay rates

$$\Gamma_a = \Gamma_b = 2\gamma(1 + \cos 2\theta), \tag{S22}$$

and the collective decay rate

$$\Gamma_{\text{coll}} = \gamma(3\cos\theta + \cos 3\theta). \tag{S23}$$

The unique geometric structure of the braided configuration enables a decoherence-free interaction between the two GAs. When $\theta = (n + 1/2)\pi$ $(n = 1, 2, 3, \ldots)$, both the individual and collective dissipation rates vanish, while the exchange coupling strength remains non-zero. This occurs because, under this phase condition, all photon emission paths that lead to the GAs' individual and collective dissipation undergo complete destructive interference. From Fig. S5, we can see that the paths causing dissipation include:

(a) four routes in the right-propagating direction: $x_{a1} \to x_{b1} \to x_{a2} \to x_{b2} \to$ far field (accumulated phase 3θ), $x_{a2} \to x_{b2} \to$ far field (accumulated phase θ), $x_{b1} \to x_{a2} \to x_{b2} \to$ far field (accumulated phase 2θ), and $x_{b2} \to$ far field (accumulated phase 0);

(b) four routes in the left-propagating direction: $x_{b2} \to x_{a2} \to x_{b1} \to x_{a1} \to$ far field (accumulated phase 3θ), $x_{b1} \to x_{a1} \to$ far field (accumulated phase θ), $x_{a2} \to x_{b1} \to x_{a1} \to$ far field (accumulated phase 2θ), and $x_{a1} \to$ far field (accumulated phase 0).

When $\theta = (n + 1/2)\pi$ $(n = 1, 2, 3, \ldots)$, the four paths traveling in the same direction satisfy the condition for destructive interference in pairs (i.e., their phase difference is an odd multiple of π), thereby making both the individual and collective dissipation rates zero.

In contrast, when $\theta = (n + 1/2)\pi$ $(n = 1, 2, 3, \ldots)$, the photon emission paths that mediate the interaction do not all undergo destructive interference. The paths mediating the interaction between the GAs include:

(a) four routes in the right-propagating direction: $x_{a1} \to x_{b1}$ (accumulated phase θ), $x_{a1} \to x_{b1} \to x_{a2} \to x_{b2}$ (accumulated phase 3θ), $x_{a2} \to x_{b2}$ (accumulated phase θ), and $x_{b1} \to x_{a2}$ (accumulated phase θ);

(b) four routes in the left-propagating direction: $x_{b2} \to x_{a2}$ (accumulated phase θ), $x_{b2} \to x_{a2} \to x_{b1} \to x_{a1}$ (accumulated phase 3θ), $x_{b1} \to x_{a1}$ (accumulated phase θ), and $x_{a2} \to x_{b1}$ (accumulated phase θ).

Since the four paths in the different directions cannot satisfy the phase condition for pairwise destructive interference, a waveguide-mediated exchange interaction still exists between the two GAs.

B. Separated GAs

For two separated GAs (see in Fig. S6), the components of SLH triplet for the right and left propagating field are

$$\begin{aligned}
S_R &= e^{3i\theta}, \\
L_R &= \Big(e^{3i\theta}\sqrt{\frac{\gamma_1^a}{2}} + e^{2i\theta}\sqrt{\frac{\gamma_2^a}{2}}\Big)\sigma_-^a + (e^{i\theta}\sqrt{\frac{\gamma_1^b}{2}} + \sqrt{\frac{\gamma_2^b}{2}})\sigma_-^b \\
H_R &= \Big(\frac{\omega_a}{2} + \frac{\sqrt{\gamma_1^a\gamma_2^a}}{4}\sin\theta\Big)\sigma_z^a + \Big(\frac{\omega_b}{2} + \frac{\sqrt{\gamma_1^b\gamma_2^b}}{4}\sin\theta\Big)\sigma_z^b \\
&\quad + \frac{1}{4i}\Big[\Big(e^{3i\theta}\sqrt{\gamma_1^a\gamma_2^b} + e^{2i\theta}\sqrt{\gamma_2^a\gamma_2^b} + e^{2i\theta}\sqrt{\gamma_1^a\gamma_1^b} + e^{i\theta}\sqrt{\gamma_2^a\gamma_1^b}\Big)\sigma_-^a\sigma_+^b - \text{H.c.}\Big],
\end{aligned} \tag{S24}$$

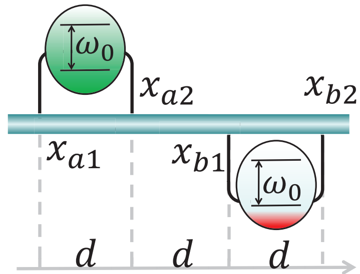

FIG. S6. Two separated GAs in the open waveguide.

and

$$
\begin{aligned}
S_L &= e^{3i\theta}, \\
L_L &= \Big(e^{i\theta}\sqrt{\frac{\gamma_2^a}{2}}+\sqrt{\frac{\gamma_1^a}{2}}\Big)\sigma_-^a+\Big(e^{3i\theta}\sqrt{\frac{\gamma_2^b}{2}}+e^{2i\theta}\sqrt{\frac{\gamma_1^b}{2}}\Big)\sigma_-^b, \\
H_L &= \Big(\frac{\sqrt{\gamma_1^a\gamma_2^a}}{4}\sin\theta\Big)\sigma_z^a+\Big(\frac{\sqrt{\gamma_1^b\gamma_2^b}}{4}\sin\theta\Big)\sigma_z^b \\
&\quad+\frac{1}{4i}\Big[\Big(e^{3i\theta}\sqrt{\gamma_1^a\gamma_2^b}+e^{2i\theta}\sqrt{\gamma_1^a\gamma_1^b}+e^{2i\theta}\sqrt{\gamma_2^a\gamma_2^b}+e^{i\theta}\sqrt{\gamma_2^a\gamma_1^b}\Big)\sigma_+^a\sigma_-^b-\mathrm{H.c.}\Big],
\end{aligned}
\tag{S25}
$$

respectively. Therefore, the components of the total triplet for the system are

$$
\begin{aligned}
S_{\mathrm{total}} &= \begin{bmatrix} e^{3i\theta} & 0 \\ 0 & e^{3i\theta} \end{bmatrix}, \\
L_{\mathrm{total}} &= \begin{bmatrix} \Big(e^{3i\theta}\sqrt{\frac{\gamma_1^a}{2}}+e^{2i\theta}\sqrt{\frac{\gamma_2^a}{2}}\Big)\sigma_-^a+(e^{i\theta}\sqrt{\frac{\gamma_1^b}{2}}+\sqrt{\frac{\gamma_2^b}{2}})\sigma_-^b \\ \Big(e^{i\theta}\sqrt{\frac{\gamma_2^a}{2}}+\sqrt{\frac{\gamma_1^a}{2}}\Big)\sigma_-^a+\Big(e^{3i\theta}\sqrt{\frac{\gamma_2^b}{2}}+e^{2i\theta}\sqrt{\frac{\gamma_1^b}{2}}\Big)\sigma_-^b \end{bmatrix}, \\
H_{\mathrm{total}} &= \Big(\frac{\omega_a}{2}+\frac{\sqrt{\gamma_1^a\gamma_2^a}}{2}\sin\theta\Big)\sigma_z^a+\Big(\frac{\omega_b}{2}+\frac{\sqrt{\gamma_1^b\gamma_2^b}}{2}\sin\theta\Big)\sigma_z^b \\
&\quad+\frac{1}{2}\Big(\sqrt{\gamma_1^a\gamma_2^b}\sin 3\theta+\sqrt{\gamma_2^a\gamma_2^b}\sin 2\theta+\sqrt{\gamma_1^a\gamma_1^b}\sin 2\theta+\sqrt{\gamma_2^a\gamma_1^b}\sin\theta\Big)(\sigma_-^a\sigma_+^b+\sigma_+^a\sigma_-^b).
\end{aligned}
\tag{S26}
$$

If we assume equal relaxation rates at all coupling points ($\gamma_1^a=\gamma_2^a=\gamma_1^b=\gamma_2^b=\gamma$), we can obtain the Lamb shifts

$$\delta\omega_a=\delta\omega_b=\gamma\sin\theta, \tag{S27}$$

the exchanging coupling strength

$$g_{ab}=\gamma(\sin\theta+2\sin 2\theta+\sin 3\theta)/2, \tag{S28}$$

the individual decay rates

$$\Gamma_a=\Gamma_b=2\gamma(1+\cos\theta), \tag{S29}$$

and the collective decay rate

$$\Gamma_{\mathrm{coll}}=\gamma(\cos\theta+2\cos 2\theta+\cos 3\theta). \tag{S30}$$

C. Nested GAs

For two nested GAs (see in Fig. S7), the components of SLH triplet for the right and left propagating field are

$$
\begin{aligned}
S_R &= e^{3i\theta}, \\
L_R &= \Big(e^{3i\theta}\sqrt{\frac{\gamma_1^a}{2}} + \sqrt{\frac{\gamma_2^a}{2}}\Big)\sigma_-^a + \Big(e^{2i\theta}\sqrt{\frac{\gamma_1^b}{2}} + e^{i\theta}\sqrt{\frac{\gamma_2^b}{2}}\Big)\sigma_-^b \\
H_R &= \Big(\frac{\omega_a}{2} + \frac{\sqrt{\gamma_1^a\gamma_2^a}}{4}\sin 3\theta\Big)\sigma_z^a + \Big(\frac{\omega_b}{2} + \frac{\sqrt{\gamma_1^b\gamma_2^b}}{4}\sin\theta\Big)\sigma_z^b \\
&\quad + \frac{1}{4i}\left\{\Big[\Big(e^{i\theta}\sqrt{\gamma_1^a\gamma_1^b} + e^{2i\theta}\sqrt{\gamma_1^a\gamma_2^b}\Big)\sigma_-^a\sigma_+^b + \Big(e^{2i\theta}\sqrt{\gamma_1^b\gamma_2^a} + e^{i\theta}\sqrt{\gamma_2^a\gamma_2^b}\sigma_+^a\sigma_-^b\Big)\Big] - \text{H.c.}\right\},
\end{aligned} \tag{S31}
$$

and

$$
\begin{aligned}
S_L &= e^{3i\theta}, \\
L_L &= \Big(\sqrt{\frac{\gamma_1^a}{2}} + e^{3i\theta}\sqrt{\frac{\gamma_2^a}{2}}\Big)\sigma_-^a + \Big(e^{i\theta}\sqrt{\frac{\gamma_1^b}{2}} + e^{2i\theta}\sqrt{\frac{\gamma_2^b}{2}}\Big)\sigma_-^b \\
H_L &= \Big(\frac{\sqrt{\gamma_1^a\gamma_2^a}}{4}\sin 3\theta\Big)\sigma_z^a + \Big(\frac{\sqrt{\gamma_1^b\gamma_2^b}}{4}\sin\theta\Big)\sigma_z^b \\
&\quad + \frac{1}{4i}\left\{\Big[\Big(e^{2i\theta}\sqrt{\gamma_1^b\gamma_2^a} + e^{i\theta}\sqrt{\gamma_2^a\gamma_2^b}\Big)\sigma_-^a\sigma_+^b + \Big(e^{i\theta}\sqrt{\gamma_1^a\gamma_1^b} + e^{2i\theta}\sqrt{\gamma_1^a\gamma_2^b}\Big)\sigma_+^a\sigma_-^b\Big] - \text{H.c.}\right\},
\end{aligned} \tag{S32}
$$

respectively. Therefore, the components of the total triplet for the system are

$$
\begin{aligned}
S_{\text{total}} &= \begin{bmatrix} e^{3i\theta} & 0 \\ 0 & e^{3i\theta} \end{bmatrix}, \\
L_{\text{total}} &= \begin{bmatrix} \Big(e^{3i\theta}\sqrt{\frac{\gamma_1^a}{2}} + \sqrt{\frac{\gamma_2^a}{2}}\Big)\sigma_-^a + \Big(e^{2i\theta}\sqrt{\frac{\gamma_1^b}{2}} + e^{i\theta}\sqrt{\frac{\gamma_2^b}{2}}\Big)\sigma_-^b \\ \Big(\sqrt{\frac{\gamma_1^a}{2}} + e^{3i\theta}\sqrt{\frac{\gamma_2^a}{2}}\Big)\sigma_-^a + \Big(e^{i\theta}\sqrt{\frac{\gamma_1^b}{2}} + e^{2i\theta}\sqrt{\frac{\gamma_2^b}{2}}\Big)\sigma_-^b \end{bmatrix}, \\
H_{\text{total}} &= \Big(\frac{\omega_a}{2} + \frac{\sqrt{\gamma_1^a\gamma_2^a}}{2}\sin 3\theta\Big)\sigma_z^a + \Big(\frac{\omega_b}{2} + \frac{\sqrt{\gamma_1^b\gamma_2^b}}{2}\sin\theta\Big)\sigma_z^b \\
&\quad + \frac{1}{2}\Big(\sqrt{\gamma_1^a\gamma_1^b}\sin\theta + \sqrt{\gamma_1^a\gamma_2^b}\sin 2\theta + \sqrt{\gamma_1^b\gamma_2^a}\sin 2\theta + \sqrt{\gamma_2^a\gamma_2^b}\sin\theta\Big)(\sigma_-^a\sigma_+^b + \sigma_+^a\sigma_-^b).
\end{aligned} \tag{S33}
$$

If we assume equal relaxation rates at all coupling points ($\gamma_1^a = \gamma_2^a = \gamma_1^b = \gamma_2^b = \gamma$), we can obtain the Lamb shifts

$$
\begin{aligned}
\delta\omega_a &= \gamma\sin 3\theta, \\
\delta\omega_b &= \gamma\sin\theta,
\end{aligned} \tag{S34}
$$

the exchanging coupling strength

$$
g_{ab} = \gamma(\sin\theta + \sin 2\theta), \tag{S35}
$$

the individual decay rates

$$
\Gamma_a = 2\gamma(1+\cos 3\theta), \Gamma_b = 2\gamma(1+\cos\theta),
$$

and the collective decay rate

$$
\Gamma_{\text{coll}} = 2\gamma(\cos\theta + \cos 2\theta). \tag{S36}
$$

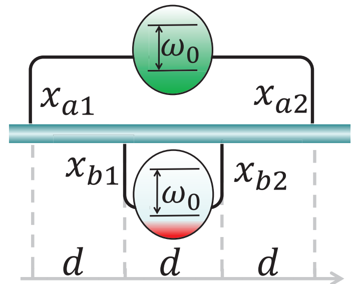

FIG. S7. Two nested GAs in the open waveguide.

D. Separated GAs in the remote chiral charging protocol

In the remote chiral charging protocol, the two separated GAs act as a charger and a battery (see in Fig. S8), respectively. The phase $\theta_{1,2}^{a(b)}$ are introduced by the external modulating signals. The distance between the charger and the battery is defined as $L = x_{b1} - x_{a2}$. For this configuration, the SLH triplet of each coupling point is

$$\begin{aligned} G_{R,1}^{a(b)} &= \Big(1, \sqrt{\tfrac{\gamma_1^{a(b)}}{2}}\sigma_-^{a(b)}, \tfrac{\omega_{a(b)}}{2}\sigma_z^{a(b)}\Big), \\ G_{R,2}^{a(b)} &= \Big(1, e^{-i\theta^{a(b)}}\sqrt{\tfrac{\gamma_2^{a(b)}}{2}}\sigma_-^{a(b)}, 0\Big), \\ G_{L,1}^{a(b)} &= \Big(1, \sqrt{\tfrac{\gamma_1^{a(b)}}{2}}\sigma_-^{a(b)}, 0\Big), \\ G_{L,2}^{a(b)} &= \Big(1, e^{-i\theta^{a(b)}}\sqrt{\tfrac{\gamma_2^{a(b)}}{2}}\sigma_-^{a(b)}, 0\Big), \end{aligned} \tag{S37}$$

where $\theta^{a(b)} = \theta_2^{a(b)} - \theta_1^{a(b)}$ are the relative phase differences. Denoting $\theta_L = k_0 L$ as the propagating phase between the two GAs, the SLH triplet for the interaction with the right propagating field is derived from the series product relation

$$G_{\mathrm{R}} = G_{\mathrm{R},2}^b \triangleleft G_\theta \triangleleft G_{\mathrm{R},1}^b \triangleleft G_{\theta_L} \triangleleft G_{\mathrm{R},2}^a \triangleleft G_\theta \triangleleft G_{\mathrm{R},1}^a, \tag{S38}$$

and the components of SLH triplet for the right propagating field are

$$\begin{aligned} S_R &= e^{i(2\theta+\theta_L)}, \\ L_R &= e^{i\theta_L}\Big(e^{2i\theta}\sqrt{\frac{\gamma_1^a}{2}} + e^{i(\theta-\theta^a)}\sqrt{\frac{\gamma_2^a}{2}}\Big)\sigma_-^a + (e^{i\theta}\sqrt{\frac{\gamma_1^b}{2}} + e^{-i\theta^b}\sqrt{\frac{\gamma_2^b}{2}})\sigma_-^b \\ H_R &= \Big[\frac{\omega_a}{2} + \frac{\sqrt{\gamma_1^a\gamma_2^a}}{2}\sin(\theta+\theta^a)\Big]\sigma_z^a + \Big[\frac{\omega_b}{2} + \frac{\sqrt{\gamma_1^b\gamma_2^b}}{2}\sin(\theta+\theta^b)\Big]\sigma_z^b \\ &\quad + \frac{1}{4i}\Big[\Big(e^{i(2\theta+\theta_L+\theta^b)}\sqrt{\gamma_1^a\gamma_2^b} + e^{i(\theta+\theta_L+\theta^b-\theta^a)}\sqrt{\gamma_2^a\gamma_2^b} + e^{i(\theta+\theta_L)}\sqrt{\gamma_1^a\gamma_1^b} + e^{i(\theta_L-\theta^a)}\sqrt{\gamma_2^a\gamma_1^b}\Big)\sigma_-^a\sigma_+^b - \mathrm{H.c.}\Big] \end{aligned} \tag{S39}$$

Similarly, the components of SLH triplet for the left propagating field are

$$\begin{aligned} S_L &= e^{i(2\theta+\theta_L)}, \\ L_L &= \Big(e^{i(\theta-\theta^a)}\sqrt{\frac{\gamma_2^a}{2}} + \sqrt{\frac{\gamma_1^a}{2}}\Big)\sigma_-^a + e^{i\theta_L}\Big(e^{i(2\theta-\theta^b)}\sqrt{\frac{\gamma_2^b}{2}} + e^{i\theta}\sqrt{\frac{\gamma_1^b}{2}}\Big)\sigma_-^b, \\ H_L &= \Big[\frac{\sqrt{\gamma_1^a\gamma_2^a}}{2}\sin(\theta-\theta^a)\Big]\sigma_z^a + \Big[\frac{\sqrt{\gamma_1^b\gamma_2^b}}{2}\sin(\theta-\theta^b)\Big]\sigma_z^b \\ &\quad + \frac{1}{4i}\Big[\Big(e^{i(2\theta+\theta_L-\theta^b)}\sqrt{\gamma_1^a\gamma_2^b} + e^{i(\theta+\theta_L)}\sqrt{\gamma_1^a\gamma_1^b} + e^{i(\theta+\theta_L+\theta^a-\theta^b)}\sqrt{\gamma_2^a\gamma_2^b} + e^{i(\theta_L+\theta^a)}\sqrt{\gamma_2^a\gamma_1^b}\Big)\sigma_+^a\sigma_-^b - \mathrm{H.c.}\Big] \end{aligned} \tag{S40}$$

Therefore, the components of the total triplet for the system are

$$
\begin{aligned}
S_{\text{total}} &= \begin{bmatrix} e^{i(2\theta+\theta_L)} & 0 \\ 0 & e^{i(2\theta+\theta_L)} \end{bmatrix}, \\
L_{\text{total}} &= \begin{bmatrix} e^{i\theta_L}\left(e^{2i\theta}\sqrt{\frac{\gamma_1^a}{2}} + e^{i(\theta-\theta^a)}\sqrt{\frac{\gamma_2^a}{2}}\right)\sigma_-^a + (e^{i\theta}\sqrt{\frac{\gamma_1^b}{2}} + e^{-i\theta^b}\sqrt{\frac{\gamma_2^b}{2}})\sigma_-^b \\ \left(e^{i(\theta-\theta^a)}\sqrt{\frac{\gamma_2^a}{2}} + \sqrt{\frac{\gamma_1^a}{2}}\right)\sigma_-^a + e^{i\theta_L}\left(e^{i(2\theta-\theta^b)}\sqrt{\frac{\gamma_2^b}{2}} + e^{i\theta}\sqrt{\frac{\gamma_1^b}{2}}\right)\sigma_-^b \end{bmatrix}, \\
H_{\text{total}} &= \left\{\frac{\omega_a}{2} + \sqrt{\gamma_1^a\gamma_2^a}\Big[\sin(\theta+\theta^a) + \sin(\theta-\theta^a)\Big]\right\}\sigma_z^a + \left\{\frac{\omega_a}{2} + \sqrt{\gamma_1^b\gamma_2^b}\Big[\sin(\theta+\theta^b) + \sin(\theta-\theta^b)\Big]\right\}\sigma_z^b \\
&\quad + \frac{1}{2}\Big[e^{i\theta^b}\sin(2\theta+\theta_L)\sqrt{\gamma_1^a\gamma_2^b} + \sin(\theta+\theta_L)\sqrt{\gamma_1^a\gamma_1^b} + e^{i(\theta^b-\theta^a)}\sin(\theta+\theta_L)\sqrt{\gamma_{2a}\gamma_2^b} \\
&\quad + e^{-i\theta^a}\sin\theta_L\sqrt{\gamma_2^a\gamma_1^b}\Big](\sigma_-^a\sigma_+^b + \sigma_+^a\sigma_-^b).
\end{aligned} \tag{S41}
$$

In the chiral charging protocol, when the relative phase $\theta_{1,2}^{a(b)}$ satisfy the following conditions:

$$\theta^a = \theta^b, \quad \theta - \theta^a = (2N+1)\pi.$$

In this case, the total triplet for the system contains only the right propagating modes (i.e. $L_L = 0$ and $H_L = 0$) when we assume equal relaxation rates at all coupling points ($\gamma_1^a = \gamma_2^a = \gamma_1^b = \gamma_2^b = \gamma$). Note that the phase term $e^{i(\theta+\theta_L)}$ can be neglected when the distance L between the two GAs is much smaller than the photon's wave packet length. This means we neglect the delay effect caused by the photon propagation between the two GAs, and we assume that the system's density matrix satisfies $\rho(t-\tau) = \rho(t)$, where $\tau \approx L/v_g$ (v_g is the photon's group velocity in the waveguide and L is the physical distance between the two GAs) represents the time required for the photon to travel between the two GAs [S4]. When L is much greater than the photon's wave packet length, we can compensate for the effect of the delay time on energy transfer by adjusting the time parameter τ in the dissipation signal. Therefore, we can obtain that

$$
\begin{aligned}
L_R &= S_a + S_b, \\
S_i &= 2i\sin\theta\sqrt{\frac{\gamma}{2}}\sigma_-^j, \quad j = a, b,
\end{aligned} \tag{S42}
$$

and

$$H_{\text{eff}} = \frac{1}{2}(\omega_a - \sin 2\theta)\sigma_z^a + \frac{1}{2}(\omega_b - \sin 2\theta)\sigma_z^b + \frac{i}{2}(S_a^\dagger S_b - \text{H.c.}). \tag{S43}$$

Therefore, we get the corresponding Lamb shifts

$$\delta\omega_a = \delta\omega_b = -\gamma_{a(b)}(t)\sin 2\theta \tag{S44}$$

in the main text as well as the exchange coupling strengths

$$g_{ab} = 2i\sqrt{\gamma_a(t)\gamma_b(t)/2}\sin^2\theta \tag{S45}$$

and the master equation

$$\dot{\rho}_I = -i[H_{\text{eff}}, \rho_I] + D[L_R]. \tag{S46}$$

S4. ANALYSIS OF ENERGY TRANSFER PROCESSES IN CHIRAL CHARGING PROTOCOL

In remote chiral charging protocol, the intial state of the giant-atom-waveguide system is assumed to be

$$|\psi(t_i)\rangle = |e_a\rangle \otimes |0_{wg}\rangle \otimes |g_b\rangle\,, \tag{S47}$$

where atom a (b) is in the excited (ground) state, and $|0_{wg}\rangle$ represents the waveguide in its vacuum state. The ideal final state should be

$$|\psi(t_f)\rangle = |g_a\rangle \otimes |0_{wg}\rangle \otimes |e_b\rangle\,. \tag{S48}$$

However, in experiment, incoherent processes, such as single-photon loss, can degrade the transfer fidelity. Therefore, the state of the system at t is expressed as [S5]

$$|\psi_t\rangle = \mu_g(t)e^{i\Phi_+(t)}|g_a g_b 0_{wg}\rangle + \left[\mu_a(t)e^{-i\Phi_-(t)}|e_a g_b 0_{wg}\rangle + \mu_b(t)e^{i\Phi_-(t)}|g_a e_b 0_{wg}\rangle + \sum_k \alpha_k(t)|g_a g_b 1_{wg}\rangle\right], \tag{S49}$$

where

$$\Phi_\pm(t) = \frac{1}{2}\int_{t_i}^{t}\omega_a^{\text{eff}}(t')dt' \pm \frac{1}{2}\int_{t_i}^{t}\omega_b^{\text{eff}}(t')dt' \tag{S50}$$

are the dynamical phases. Time-dependent frequency shifts due to Lamb shifts are incorporated into the effective atomic frequency $\omega_{a(b)}^{\text{eff}}$ [S6]. In the following discussion, the numerical simulation is confined to the single-excitation subspace, i.e., $\mu_g(t) = 0$, which simplifies the problem by eliminating the unknown dynamical phase. Note that α_k denotes the probability of excitation leaking into the mode k of the waveguide. To minimize this leakage, the system's evolution can be controlled to satisfy the following dark state condition

$$[S_a(t) + S_b(t)]\,|\psi_t\rangle = 0, \tag{S51}$$

which restricts the evolution and time-dependent decay rates satisfying the following relation

$$\sqrt{\Gamma_a(t)}\mu_a(t) + \sqrt{\Gamma_b(t)}\mu_b(t) = 0, \tag{S52}$$

where $\Gamma_{a(b)}(t)$ are defined as $\Gamma_{a(b)}(t) = 4(\sin\theta)^2\gamma_{a(b)}(t)$. By combining equations (S43) and (S52), one can obtain the evolution functions $\mu_{a(b)}(t)$ as

$$\dot{\mu_a}(t) = -\frac{\Gamma_a(t)}{2}\mu_a(t), \tag{S53}$$

$$\dot{\mu_b}(t) = -\frac{\Gamma_b(t)}{2}\mu_b(t) - \sqrt{\Gamma_a(t)\Gamma_b(t)}\mu_a(t). \tag{S54}$$

The perfect energy transfer requires the intial and final states satisfying the boundary conditions:

$$\mu_a(t_i) = \mu_b(t_f) = 1, \quad \mu_a(t_f) = \mu_b(t_i) = 0. \tag{S55}$$

To find suitable dissipation sequences, we make use of the following time symmetry argument: if a photon is emitted by one qubit, then, upon reversing the direction of time, we would see a perfect reabsorption. Based on this, we must ensure that the emitted photon shape remains invariant under time reversal, and we use a time-reversed control pulse for the second qubit [S6].

In the charging protocol, the photon shape in the waveguide can be defined as $a(t) = \sqrt{\Gamma_a}\mu_a$. We can ensure that its time derivative satisfies $\dot{a}(t) = f(t)a$ through a series of pulses, where $f(t)$ satisfies the condition $f(t) = -f(-t)$, thereby ensuring that the photon absorption process of the second GA is the time-reversed copy of the photon emission process of the first GA. For the sake of discussion, we assume $t_f = -t_i$ here.

From Eq. (S53), we can obtain

$$\dot{a} = \frac{d}{dt}(\sqrt{\Gamma_a}\mu_a) = \frac{1}{2}\frac{\dot{\Gamma}_a}{\sqrt{\Gamma_a}}\mu_a - \frac{\Gamma_a}{2}\sqrt{\Gamma_a}\mu_a \tag{S56}$$

Substituting $\mu_a = a/\sqrt{\Gamma_a}$ into the above equation, it becomes

$$\dot{a} = \left(\frac{1}{2}\frac{\dot{\Gamma}_a}{\Gamma_a} - \frac{\Gamma_a}{2}\right)a. \tag{S57}$$

Therefore, we have

$$\begin{aligned}\left(\frac{1}{2}\frac{\dot{\Gamma}_a}{\Gamma_a} - \frac{\Gamma_a}{2}\right) &= f(t)\\ \dot{\Gamma}_a &= \Gamma_a^2 + 2f(t)\Gamma_a.\end{aligned} \tag{S58}$$

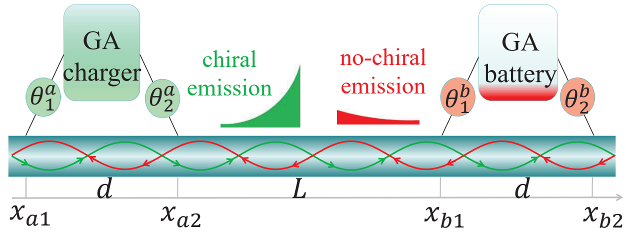

FIG. S8. Schematic diagram of remote chiral charging protocol.

The dissipation sequence satisfying this differential equation ensures that the photon shape emitted by GA a is time-reversed.

Once a positive and bounded solution is obtained from Eq. (S58), we can use it to calculate $\mu_a(t)$. The quantities in GA b are then given by $\mu_b(t) = -\mu_a(-t)$ and $\Gamma_b(t) = \Gamma_a(-t)$.

It can be verified that when $f(t) = -\Gamma_{\max}\text{sgn}(t)/2$, a solution of Eq. (S58) is given by

$$\Gamma_a(t<0) = \Gamma_{\max}\frac{e^{\Gamma_{\max}t}}{2-e^{\Gamma_{\max}t}}, \quad \Gamma_a(t \geq 0) = \Gamma_{\max}. \tag{S59}$$

The dissipation sequence in Eq. (S59) theoretically and perfectly satisfies the dark state condition:

$$\sqrt{\Gamma_a(t)}\mu_a(t) + \sqrt{\Gamma_b(t)}\mu_b(t) = \sqrt{\Gamma_a(t)}\mu_a(t) - \sqrt{\Gamma_a(-t)}\mu_a(-t) = 0, \tag{S60}$$

ensuring the lossless transfer of energy between the GAs.

When considering the delay effect caused by photon propagation, the pulse sequence becomes:

$$\Gamma_a(t) = \Gamma_b(\tau - t) = \begin{cases} \dfrac{\Gamma_{\max}e^{\Gamma_{\max}(t-\tau)}}{2-e^{\Gamma_{\max}(t-\tau)}}, & t < \tau \\ \Gamma_{\max}, & t \geq \tau \end{cases} \tag{S61}$$

In experiments, the decay sequences of two GAs can be realized by designing time-dependent coupling strength at each connection point, which corresponds to changing the amplitude of control flux. Taking GA a as an example, the decay rate [S4] is

$$\Gamma_a = \frac{L_{wg}}{2v_g}(|g_{k_r}|^2 + |g_{-k_r}|^2), \tag{S62}$$

where L_{wg} is the waveguide total length, v_g is the group velocity, and $g_{\pm k_r}$ are the coupling strength of the atom with the right-/left-propagating wave vector $\pm k_r$ When the phase condition is satisfied, g_{-k_r} becomes zero. In the next section, we will demonstrate how to design the time-dependent coupling strength by adjusting the amplitude of the magnetic flux.

S5. TIME-DEPENDENT COUPLING BETWEEN SUPERCONDUCTING GAS AND THE WAVEGUIDE

Figure S9 shows that a superconducting GA interacts with the waveguide at two points. Each coupling point is mediated by a Josephson junction inserted in a loop.The inductance $\mathcal{L}_{wi}$ and $\mathcal{L}_{qi}$ of the ith loop (i=1,2) are the shared branch in the waveguide and GAs, respectively. The phase difference across Josephson inductance in loop i is denoted as ϕ_J^i. The intermediate junction can be viewed as a lumped inductance $\mathcal{L}_i$ as

$$\mathcal{L}_i = \frac{\mathcal{L}_T}{\cos\phi_J^i}, \quad \mathcal{L}_T = \frac{\Phi_0}{2\pi I_c} \tag{S63}$$

where I_c represents the critical currents of two junctions. Note that $\mathcal{L}_{wi}$, $\mathcal{L}_{qi}$, and $\mathcal{L}_i$ form the loop C_i at the ith coupling point, through which an external flux bias $\Phi_{\text{ext}}^{(i)}$ is applied. We assume that the inductance branch $\mathcal{L}_{wi}(\mathcal{L}_{qi})$

is much smaller than the total inductance of the atom (the waveguide). The boundary relation of the loop C_i is given by [S7]

$$\phi_J^{(i)} = \int \mathbf{A}d\mathbf{l} = \frac{2\pi}{\Phi_0}\Big[\Phi_{\rm ext}^{(i)} - (\mathcal{L}_{wi}+\mathcal{L}_{qi})I_c \sin\phi_J^{(i)}\Big]. \tag{S64}$$

One can find that $\phi_J^{(i)}$ is restricted by the following transcendental equation

$$\phi_J^{(i)} + \frac{\mathcal{L}_{wi}+\mathcal{L}_{qi}}{\mathcal{L}_T}\sin\phi_J^{(i)} = \frac{2\pi}{\Phi_0}\Phi_{\rm ext}^{(i)}, \tag{S65}$$

which shows that $\phi_J^{(i)}$ can be controlled by the external flux. We set $\beta = (\mathcal{L}_{wi}+L_{qi})/\mathcal{L}_T$ and assume $\mathcal{L}_{wi} = \mathcal{L}_{qi} = \mathcal{L}_0$. By applying the $Y-\Delta$ transformation for the coupling loop, the effective mutual inductance between the waveguide and the GA is derived as [S8]

$$M_{gi} = \frac{\mathcal{L}_0^2}{2\mathcal{L}_0+\mathcal{L}_i} = \frac{\mathcal{L}_0^2}{\mathcal{L}_T}\frac{\cos\phi_J^i}{1+\beta\cos\phi_J^i}. \tag{S66}$$

Therefore, the mutual inductance M_{gi} is tunable by changing the external flux $\Phi_{\rm ext}^{(i)}$. The modulating relation is found from the transcendental equations (S65) and (S66). By assuming $\beta \ll 1$, we obtain $\phi_J^{(i)} \approx \frac{2\pi}{\Phi_0}\Phi_{\rm ext}^{(i)}$ and derive the effective mutual inductance as

$$M_{gi} = \frac{\mathcal{L}_0^2}{\mathcal{L}_T}\cos\Big(\frac{2\pi}{\Phi_0}\Phi_{\rm ext}^{(i)}\Big), \tag{S67}$$

which shows that the mutual indutance M_{gi} can be modulated by $\Phi_{\rm ext}^{(i)}$ in a cosine form.

Given that the transmon is of weak Kerr nonlinearity, we can approximately view it as a Duffing oscillator, which quantization Hamiltonian is

$$H_q = \hbar\Omega_q b^\dagger b - \frac{E_C}{12}(b+b^\dagger)^4, \tag{S68}$$

where $\Omega_q = \frac{1}{\sqrt{\mathcal{L}_Q C_q}}$, $\mathcal{L}_Q$ is the total inductance of the transmon, C_q is the total transmon capacitance, $E_C = e^2/(2C_Q)$ is the charge energy, and b ($b^\dagger$) is the annihilation (creation) operator. The current operator of the transmon is approximately written as [S7]

$$I_q \approx \sqrt{\frac{\hbar\Omega_q}{2\mathcal{L}_Q}}(b+b^\dagger). \tag{S69}$$

By considering two lowest energy levels, we rewrite the Hamiltonian H_q in the Pauli representation, i.e., by replacing $b^\dagger(b) \rightarrow \sigma_-(\sigma_+)$

$$H_q \approx \frac{1}{2}\hbar\omega_q\sigma_+\sigma_-, \tag{S70}$$

$$I_q = \sqrt{\frac{\hbar\Omega_q}{2\mathcal{L}_Q}}(\sigma_-+\sigma_+), \tag{S71}$$

$$\omega_q = \Omega_q - \frac{E_C}{\hbar}. \tag{S72}$$

The current operator of the waveguide is written as [S9]

$$I_w = i\sum_{l,k}\sqrt{\frac{\hbar\omega_l(k)}{2\mathcal{L}_{tot}}}\Big[a_{lk}e^{-ikx}u_{lk}^*(x) - a_{lk}^\dagger e^{ikx}u_{lk}(x)\Big], \tag{S73}$$

where $\omega_l(k)$ is the eigenfrequency of mode k in the lth energy band, $\mathcal{L}_{tot} = \mathcal{L}_{wg}l_0$ is the total inductance with $\mathcal{L}_{wg}$ being the waveguide total length and l_0 being the static inductance, a_{lk} ($a_{lk}^\dagger$) is the annihilation (creation) operators for the mode k in the lth energy band, and $u_{lk}(x)$ is the Bloch eigen-function satisfying $u_{lk}(x) = u_{lk}(x+\lambda_m)$ with

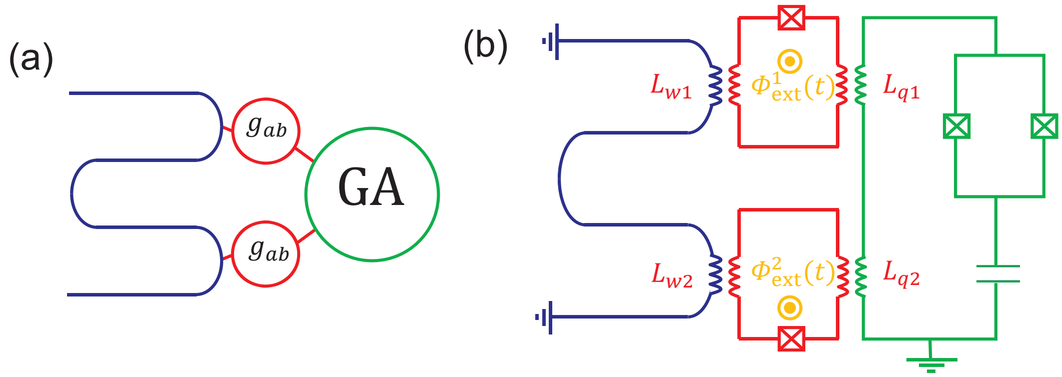

FIG. S9. Tunable coupling between the waveguide and a superconducting GA of transform form. The blue line represents a coplanar waveguide. The coupling points are mediated via loops with Josephson junctions (red crosses). At coupling point i, L_{wi} and L_{qi} are the shared branch inductances in the waveguide and the transform qubit, respectively. The time-dependent couplings can be obtained by applying an external time-dependent flux $\Phi_i(t)$.

λ_m being the periodic length. We have assumed the waveguide is a Josephson photonic-crystal waveguide. The interaction Hamiltonian between the waveguide and the GA is

$$H_I = \sum_{i=1,2} M_{gi}(t) I_q I_w \approx \hbar \sum_l \sum_k \left[g_{lk}(t) a^\dagger_{lk} \sigma_- + \text{H.c.} \right], \tag{S74}$$

$$g_{lk}(t) = \frac{1}{2}\sqrt{\frac{\omega_q \omega_l(k)}{\mathcal{L}_{tot}\mathcal{L}_Q}} \sum_{i=1,2} M_{gi}(t) e^{ikx_i} u_{lk}(x_i), \tag{S75}$$

where $M_{gi}(t) = \frac{L_0^2 \Phi_0}{2\pi I_c} \cos\left(\frac{2\pi}{\Phi_0}\Phi^i_{\rm ext}\right)$ is the effective mutual inductance and $\Phi^{(i)}_{\rm ext} = \Phi_{bi} + \frac{\Phi_0}{2\pi} d_i \cos(\Omega_d t + \phi_i)$ is the external flux with the dc part Φ_{bi} and the modulating amplitude d_i (phase ϕ_i). Assuming that d_i is small, $M_{gi}(t)$ can be simplified as $M_{gi}(t) \approx A_1 \frac{L_0^2}{L_T} \cos(\Omega_d t + \phi_i)$, where A_1 is the first order Fourier amplitude of $M_{gi}(t)$. Consequently, the time-dependent coupling between GAs and the waveguide is obtained [S4].

In the chiral charging protocol, both the phase condition $\theta - \theta^{a(b)} = (2N+1)\pi$ and the dark state condition $\sqrt{\Gamma_a(t)}\mu_a(t) + \sqrt{\Gamma_b(t)}\mu_b(t) = 0$ must be satisfied to achieve lossless unidirectional flow between the charger and the battery.The fulfillment of these two conditions requires the separate modulation of the phase and amplitude components of the external magnetic flux, respectively. Specifically, to achieve chiral emission, the phase difference between the two magnetic fluxes applied in each GA must satisfy $\phi_2 - \phi_1 = \theta_2^{a(b)} - \theta_1^{a(b)} = \theta^{a(b)} = \theta - (2N+1)\pi$. The parameters provided in Reference [S4] indicate that when the distance between the coupling points of each GA is an integer multiple of the resonant mode wavelength, the phase difference corresponding to perfect chiral emission is 0.12π. As for the dissipation rates $\Gamma_{a(b)}(t)$, we need to design appropriate magnetic flux amplitudes d_i to satisfy the dissipation sequence given in Eq. (S61). The dependence of the coupling strength on the magnetic flux amplitude is also discussed in the Appendix of Reference [S4].

If we aim to utilize the braided configuration to achieve both battery charging and energy storage, we can implement it in the following manner:

(i) Charging Phase: The system composed of braided GAs is operating at the decoherence-free point (e.g., $\theta = \pi/2$). The constant coupling g_{ab} enables the lossless, coherent energy transfer from the charger to the battery.

(ii) Storage Phase: Once the battery is fully charged (e.g., at the peak of the oscillation), the coupling between the battery (GA b) and the waveguide is dynamically tuned to zero by adjusting the external fluxes on its coupling points. This effectively decouples the battery from the waveguide, freezing its energy in the excited state without any oscillation or energy leakage. This is achieved without needing to change the propagation phase θ.

This proposed method uses dynamic control to create a zero-coupling condition at will from any initial configuration, providing the necessary on/off functionality for a practical QB. This approach does not re-introduce decoherence during the storage phase because the battery is actively decoupled from the primary dissipation channel (the waveguide).

[S1] W. Shao, C. Wu, and X.-L. Feng, Generalized James' effective Hamiltonian method, Phys. Rev. A **95**, 032124 (2017).

[S2] J. Combes, J. Kerckhoff, and M. Sarovar, The SLH framework for modeling quantum input-output networks, Adv. Phys.: X **2**, 784–888 (2017).

[S3] A. F. Kockum, G. Johansson, and F. Nori, Decoherence-free interaction between giant atoms in waveguide quantum electrodynamics, Phys. Rev. Lett. **120**, 140404 (2018).

[S4] X. Wang and H.-R. Li, Chiral quantum network with giant atoms, Quantum Sci. Technol. **7**, 035007 (2022).

[S5] J. I. Cirac, P. Zoller, H. J. Kimble, and H. Mabuchi, Quantum state transfer and entanglement distribution among distant nodes in a quantum network, Phys. Rev. Lett. **78**, 3221 (1997).

[S6] K. Stannigel, P. Rabl, A. S. Sørensen, M. D. Lukin, and P. Zoller, Optomechanical transducers for quantum-information processing, Phys. Rev. A **84**, 042341 (2011).

[S7] M. R. Geller, E. Donate, Y. Chen, M. T. Fang, N. Leung, C. Neill, P. Roushan, and J. M. Martinis, Tunable coupler for superconducting xmon qubits: Perturbative nonlinear model, Phys. Rev. A **92**, 012320 (2015).

[S8] F. Wulschner, J. Goetz, F. R. Koessel, E. Hoffmann, A. Baust, P. Eder, M. Fischer, M. Haeberlein, M. J. Schwarz, M. Pernpeintner, E. Xie, L. Zhong, C. W. Zollitsch, B. Peropadre, J.-J. Garcia Ripoll, E. Solano, K. G. Fedorov, E. P. Menzel, F. Deppe, A. Marx, and R. Gross, Tunable coupling of transmission-line microwave resonators mediated by an rf SQUID, EPJ Quantum Technol. **3** (2016).

[S9] X. Wang, T. Liu, A. F. Kockum, H.-R. Li, and F. Nori, Tunable chiral bound states with giant atoms, Phys. Rev. Lett. **126**, 043602 (2021).